

---

# Local Convolutions Cause an Implicit Bias towards High Frequency Adversarial Examples

---

Josue Ortega Caro<sup>1,2,+</sup>, Yilong Ju<sup>3</sup>, Ryan Pyle<sup>1</sup>, Sourav Dey<sup>4</sup>, Wieland Brendel<sup>5</sup>, Fabio Anselmi<sup>1</sup>, and Ankit B Patel<sup>1,6</sup>

<sup>1</sup>Department of Neuroscience, Baylor College of Medicine, Houston, TX, 77030

<sup>2</sup>Quantitative and Computational Bioscience Program, Baylor College of Medicine, Houston, TX, 77030

<sup>3</sup>Department of Computer Science, Rice University, Houston, TX, 77005

<sup>4</sup>Manifold AI

<sup>5</sup>University of Tübingen, Germany,

<sup>6</sup>Department of Electrical and Computer Engineering, Rice University, Houston, TX, 77005

<sup>+</sup>Correspondence to: caro@bcm.edu

## Abstract

Adversarial Attacks are still a significant challenge for neural networks. Recent work has shown that adversarial perturbations typically contain high-frequency features, but the root cause of this phenomenon remains unknown. Inspired by theoretical work on *linear full-width convolutional models*, we hypothesize that the *local* (i.e. *bounded-width*) *convolutional operations* commonly used in current neural networks are *implicitly* biased to learn high frequency features, and that this is one of the root causes of high frequency adversarial examples. To test this hypothesis, we analyzed the impact of different choices of linear and *nonlinear* architectures on the implicit bias of the learned features and the adversarial perturbations, in both spatial and frequency domains. We find that the high-frequency adversarial perturbations are critically dependent on the convolution operation because the spatially-limited nature of *local* convolutions induces an implicit bias towards *high* frequency features. The explanation for the latter involves the Fourier Uncertainty Principle: a spatially-limited (local in the space domain) filter cannot also be frequency-limited (local in the frequency domain). Furthermore, using larger convolution kernel sizes or avoiding convolutions (e.g. by using Vision Transformers architecture) significantly reduces this high frequency bias, but not the overall susceptibility to attacks. Looking forward, our work strongly suggests that understanding and controlling the implicit bias of architectures will be essential for achieving adversarial robustness.

## Introduction

Despite the enormous progress in training neural networks to solve hard tasks, they remain surprisingly and stubbornly sensitive to imperceptibly small worst-case perturbations known as *adversarial examples*. This lack of robustness has sparked many theories [1–9], but a unified theoretical explanation of the nature of adversarial examples is still lacking.

Recent work has shown that commonly found adversarial examples for state-of-the-art convolutional neural networks are mainly composed of high frequency information[10]. In addition, they found that adversarial perturbations of naturally trained models tend to be higher frequency as compared to those of adversarially trained models. Furthermore, Wang et al, 2020, found that high frequency features

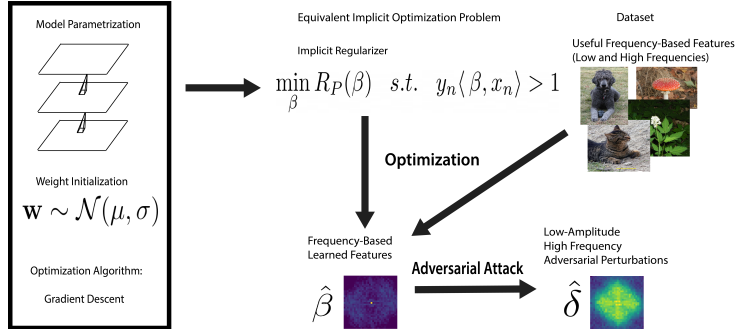


Figure 1: The Implicit Fourier Regularization (IFR) Hypothesis. Model parametrization and weight initialization induces an implicit optimization bias. This leads to different learned features  $\beta$  and therefore, different adversarial perturbations  $\delta$ . In particular, implicit regularization in the frequency domain, directly caused by the translation invariance of the convolution operation, is necessary for the evolution of frequency-based features. Furthermore, the spatially-limited nature of common local convolutional operations encourages the learned features  $\beta$  to possess energy in *higher* frequencies.

are necessary for high generalization performance of state-of-the-art convolutional models[11]. These results lead to different theories for understanding robustness and generalization of neural networks through a frequency lense. For example, Universal Adversarial Perturbations (UAPs) is a method to compute what directions in input space are neural networks sensitive to[12]. They found that convolutional neural networks were sensitive to noise in the Fourier Basis. Other work such as Neural Anisotropic Directions (NADs) found linearly separable directions for which a neural network might be able classify an input[13, 14]. This is evidence that a frequency-based understanding of model robustness might be an important step towards building robust, interpretable models. A natural question arises: *Why frequencies*, as opposed to some other basis?

Here we propose an answer to this question that relies on the concept of *implicit bias*. The idea behind implicit bias is that the loss landscape of an overparameterized network has infinitely many global minima, and which global minimum one converges to after training depends on many factors, including the choice of model architecture/parametrization [15, 16], initialization scheme [17] and optimization algorithm [18–20]. The implicit bias of state-of-the-art models has been shown to play a critical role in the generalization of deep neural networks [21, 22]. Recent theoretical work [15] on *L-layer deep linear networks* has revealed that (i) fully connected layers induce a depth-independent ridge ( $\ell_2$ ) regularizer in the spatial domain whereas, surprisingly, *full-width convolutional layers* induce a depth-dependent *sparsity* ( $\ell_{2/L}$ ) regularizer in the *frequency* domain. Linear full-width convolutional models are different from the high-performance convolutional neural networks (CNNs) used in practice. Nonetheless, we hypothesised that similar mechanisms might play a role for *deep nonlinear models with local convolutions*, meaning that the high frequency nature of commonly-found adversarial perturbations is due to the implicit bias induced by the specific architectural choice. More formally, we propose the Implicit Fourier Regularization (IFR) hypothesis (see Figure 1):

*Implicit regularization in frequency domain, directly caused by the translation invariance and spatially limited nature of bounded-width convolutions, yields a strong bias towards high frequency features and adversarial perturbations.*

The IFR hypothesis can be decomposed into three parts, and we will provide evidence for each later on in the paper. First, convolutions, due to their translation invariant nature, induce an implicit bias promoting sparsity in the Fourier domain for *nonlinear* CNNs with full-width convolutions (thereby extending theoretical results on *linear* models [15]). Second, restricting to bounded-width (spatially limited/localized) convolutions changes the implicit bias, encouraging the linear features to possess more energy in *high* frequencies; this arises because a space-limited filter cannot also be band-limited, a mathematical consequence of the Fourier Uncertainty Principle. Third, the high frequency features learned by the model in turn induce high frequency adversarial perturbations.

## Experimental Results

**Impact of Model Parametrization on Adversarial Perturbations.** Recent theoretical work [15] has shown that shallow linear convolutional neural networks ( $L$  **full-width circular** convolutional linear layers followed by one **fully connected** linear layer) induce an implicit sparsity-promoting regularizer in the Fourier domain. Specifically, the regularizer is:  $\mathcal{R}_{FWC}(\beta_L) = \|\widehat{\beta}_L\|_{\frac{2}{L}}$  where  $\widehat{\beta}_L := \mathcal{F}\beta_L$  is the Discrete Fourier Transform (DFT) of the end-to-end linear transformation  $\beta_L := \prod_i^L W_i$  represented by the linear network and  $L$  is the number of layers. If the implicit bias affects the features learned by the model, could it also alter the nature of the adversarial perturbations?

**Confirming [15] results and relationship to adversarial perturbations.** To test our hypothesis, we selected the two model parametrizations considered in [15], namely fully connected and full-width convolutional models. In addition, we used shallow (one hidden layer) and deep (three hidden layers) versions of these models, along with linear and nonlinear activation functions. These models were trained on CIFAR-10 dataset [23] (MIT) using PyTorch [24] (performance in Supp. Table 7).

Our goal here is to understand the relationship between the learned features  $\beta$  learned by these models and their corresponding adversarial perturbations  $\delta$  (See Methods for details). In Figure 2, we can see the average Fourier spectrum of the adversarial perturbations ( $\widehat{\delta}$ ) for PGD-Linf [25] and the average Fourier spectrum of the input-output weight visualization ( $\widehat{\beta}$ ). We observe that the full-width convolutional model (FWC) has a sparser spectrum of  $\beta$  compared to the fully connected model (FC), and when the model has more layers this difference increases (Deep FWC vs Deep FC). This is experimental confirmation of the theoretical result in [15] for linear models. Furthermore, to quantify the different sparsity levels of the two models, we measure the  $\ell_1$  and  $\ell_2$  norm of the Fourier spectrum of  $\beta$  for both the shallow and deep full-width and fully connected models (See Sup. Fig 6). We observe that the relationship between model parametrization and spectrum holds for the spectrum of the adversarial perturbations  $\widehat{\delta}$ , where the full-width convolutional model has a sparse adversarial spectrum compared to the fully connected model. This was confirmed quantitatively by computing their Spearman correlation (see Supp. Table 3). These results also hold for the other attacks (see Supp. Figure 8, 9).

However, in contrast with theory, which predicts that  $\delta \propto \beta$  for linear models, we instead find correlations  $< 1$  [26, 7]. This is because a successful adversarial attack requires only a minimal perturbation of the input such that the output category changes, therefore, an adversarial might not use all features directions but only a selected few. As a consequence, the correlation between  $\beta$  and  $\delta$  need not be maximal.

Next, we tested if the implicit regularizer has the same properties for nonlinear models. As we observe in Figure 2, the full-width convolutional model has a sparse spectrum of both  $\beta$  and  $\delta$  compared to the fully connected model. This shows that the implicit regularizer due to the model holds for both linear and nonlinear models.

**Expanding to Bounded-Width Convolutional Models.** One limitation of this theory is that full-width convolutional layers are not often used in common state-of-the-art architectures. Bounded-width convolutional models are instead usually employed, which have smaller kernel sizes than the width of the input. Given this, we asked: what is the effect of the bounded-width convolutional model in  $\widehat{\beta}$  and  $\widehat{\delta}$ ?

To answer this question, we trained a bounded-width convolutional model and generated both  $\widehat{\beta}$  and  $\widehat{\delta}$  with the same procedure as the previous section. In Figure 2, we can see that the bounded-width convolutional models (both linear and nonlinear) contain high frequency components in  $\widehat{\delta}$ . This is further exacerbated by depth in the Deep Bounded-Width model (DBWC). Moreover, we observe that the  $\beta$  corresponding to the bounded-width convolutional model is as sparse or less sparse (more dense) compared to the full-width counterpart (see Supp. Figure 6). Given that the theory [15] only specifies a bias towards  $\ell_{\frac{2}{L}}$ -sparsity in the frequency domain (support can consist of low or high frequencies), then why do we observe so much more concentration of energy in the higher frequencies of the bounded-width convolutional model but not the full-width convolutional model? Our experiments suggest that this is due to *the spatial locality constraint* imposed in the bounded-width convolutions. We propose a theoretical explanation via the Fourier Uncertainty Principle – a space-limited kernel

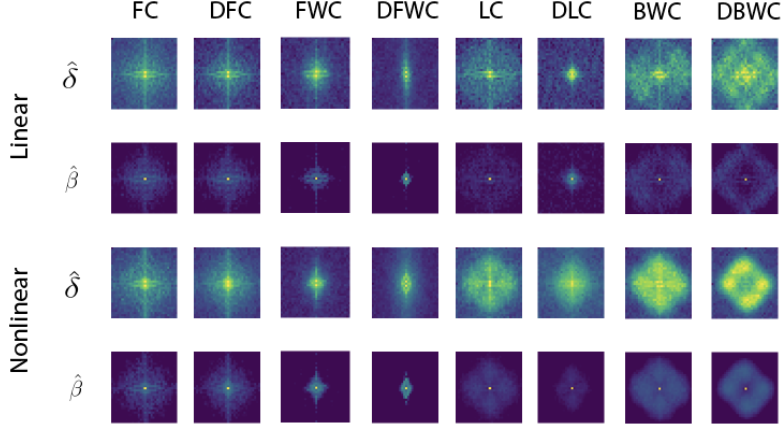


Figure 2: Average Frequency Spectrum of adversarial perturbation ( $\hat{\delta}$ ) and input-output weights ( $\hat{\beta}$ ) for Fully Connected (FC), Full-Width Convolutional (FWC), Locally Connected (LC) and Bounded-Width Convolutional (BWC) models for PGD-Linf Attack. We can observe the correlation between the input-output weights and the adversarial perturbations for each model. This results also hold for different attacks (See Sup. Figures 8, 9)

cannot be band-limited in frequency domain – as the origin of frequency dispersion. This reasoning can be made rigorous for a bounded-width linear convolutional model by a simple and straightforward extension of the results of Gunasekar et al, 2018 along with the invocation of energy concentration Uncertainty Principle. This results in the following theorem:

**Theorem 1.** *Let  $\beta := \star_{l=1}^{L-1} w_l$  be the end to end linear predictor. Then spatially concentrating the energy of each convolutional filter  $w_l \in \mathbb{R}^D$  results in an increased concentration of energy in high frequencies for  $\hat{\beta}$ .*

Here we informally present the key steps of the proof. A rigorous mathematical treatment can be found in the Appendix D. The key intuition is that, due to the Fourier Uncertainty Principle, decreasing the support of the convolutional filter  $w_l$  causes an increase of its high frequency energy content. What is the effect of this high-frequency shift on the end-to-end linear predictor  $\beta$ ? Since it is a product of convolutions, the Discrete Fourier transform of  $\beta$  is the Hadamard product of the Discrete Fourier transforms of the convolutional filters (see also Lemma 3 in Gunasekar et al, 2018). Taking the  $\ell_2$  norm of  $\beta$  and using a norm inequality on the Hadamard product finally shows that  $\|\hat{\beta}\|_2 \leq \prod_{l=1}^L \|\hat{w}_l\|_2$ . In words, decreasing the support of the per-layer convolutional filters results in an increase in the high frequencies energy content of  $\beta$ . Further, as we reduce the convolutional filters support, the result of the optimization problem for the implicit regularizer will only increase in cost, since less degrees of freedom are available for the solution. In summary, all else being equal, reducing the convolutional kernel size causes/induces a bias towards more concentration of energy in higher frequencies in  $\beta$ .

We directly tested our theory on the same models proposed by Gunasekar 2018 but with varying kernel sizes (3 by 3, 7 by 7, 11 by 11, 15 by 15, 21 by 21, and 32 by 32), with 1 or 3 hidden layers same as our original results, and train them on Grayscale CIFAR10. This was to keep the number of hidden channels equal to the number of input channels. Then we computed the frequency spectrum of  $w_l$  and the cumulative weights up to layer  $l$ ,  $\beta_l$ . Next we computed the  $\kappa_{high}$ , which is the fraction of energy outside of an interval  $[-\frac{k}{2}, +\frac{k}{2}]$  divided by the total energy for each kernel. In Supp. Figure 7a, we observe that the fraction of energy is a function of the kernel size, where for smaller  $k$   $\kappa_{high}$  is higher. Furthermore, as the model goes deeper, we can see that this difference is further exacerbated. We can observe this phenomenon both for deeper models and during training (See Supp. Figure 7b).

**Role of Translation Invariance in the frequency spectrum of  $\beta$  and  $\delta$ .** Next, to further investigate the origin of the high frequency bias, we asked: Is the effect of the bounded-width convolutional model also present in a model with only local kernels but not translation invariance (i.e. no shared weights)? For this we trained a locally connected model with same kernel size on CIFAR10. In

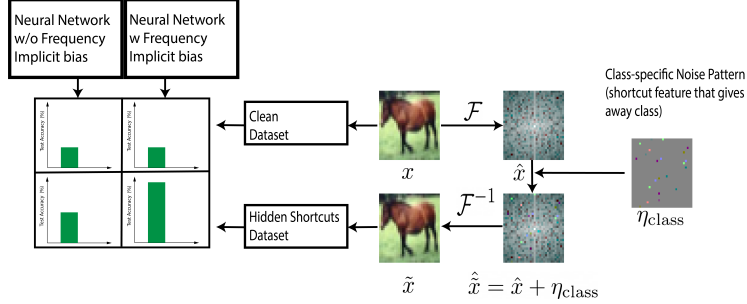


Figure 3: Steganography experiment. Class specific information  $\eta_{class}$  introduced into Fourier Spectrum of training set image ( $\tilde{x} = \hat{x} + \eta_{class} : \eta_{class} = M_{class} \odot (\epsilon * N_{class}), N_{class} \sim \mathcal{N}(0, 1), M_{class} \sim \text{Bernoulli}(\rho)$ ). Models with sparse frequency regularizer (Full-Width and Bounded-Width Convolutional models) should take more advantage of hidden shortcut features in the dataset, therefore leading to higher test accuracy.

Figure 2 we observe that the locally connected models (LC and DLC) do not have as much energy in the higher frequencies, particularly for the deep models. This shows that local connectivity alone is *not* sufficient to bias the model towards learning high frequency features; translation invariance is also required. *Thus, local convolutions are necessary to obtain bias towards high frequency features, and therefore adversarial perturbations.* Importantly, we found the same results for CIFAR100, which has image statistics similar to CIFAR10. However, we did not for MNIST, which has no useful high frequency information (See Supp. Figure 5). This shows that an interaction between the implicit bias (induced by the model parametrization) and the dataset statistics is essential for high frequency features to be learned.

**Testing different implicit bias via the Injection of Hidden Shortcut Features.** Given that the theory in Gunasekar et al, 2018 doesn't extend to the implicit regularization for nonlinear convolutional models, and our results on the relationship of  $\hat{\beta}$  and  $\hat{\delta}$ , we decided to directly test if the nonlinear bounded-width convolutional model is able to capture sparse frequency-based information in the dataset, thus confirming that the sparse implicit regularization theory also holds for nonlinear models.

To test our hypothesis, we take inspiration from the field of steganography which focuses on hiding shortcut features in images that are visually undetectable by humans [27]. We introduced a class-correlated sparse shortcut feature into every CIFAR-10 train and test set image (See Figure 3). Our hypothesis is that these class-dependent shortcut features will be mostly useful for model parametrizations that have an implicit regularizer that is sparse in the frequency domain. Therefore the model with the right implicit bias should achieve *higher* test accuracy (For generation of the shortcut features see Methods).

Table 1: Performance on CIFAR-10 on base vs frequency-based dataset , mean  $\pm$  std over 5 trials each.

	Baseline	$\epsilon = .25, \rho = .2$	$\epsilon = .25, \rho = .1$
Fully Connected Linear	40.8 $\pm$ .070	53.26 $\pm$ .075	45.27 $\pm$ 1.14
Fully Connected Nonlinear	48.5 $\pm$ .084	59.6 $\pm$ .223	54.93 $\pm$ .497
Full Width Convolutional Linear	41.8 $\pm$ .124	70.3 $\pm$ .805	79.6 $\pm$ 1.35
Full Width Convolutional Nonlinear	52.4 $\pm$ 2.89	79.5 $\pm$ .912	87.2 $\pm$ 1.26
Bounded Width Convolutional Linear	41.8 $\pm$ .046	97.28 $\pm$ .604	92.33 $\pm$ .679
Bounded Width Convolutional Nonlinear	56.7 $\pm$ .489	98.8 $\pm$ .850	97.8 $\pm$ .475

Table 1 shows the test accuracy of each linear and nonlinear model with the new dataset and different levels of sparsity. We can observe that both the full-width and bounded-width models have higher performance than baseline with this new dataset. However, the fully connected model, having a different bias, cannot take full advantage of the class-dependent shortcut feature introduced into the dataset. This experiment reveals that the implicit regularizer for sparsity in the frequency domain is present in both linear and nonlinear convolutional models.

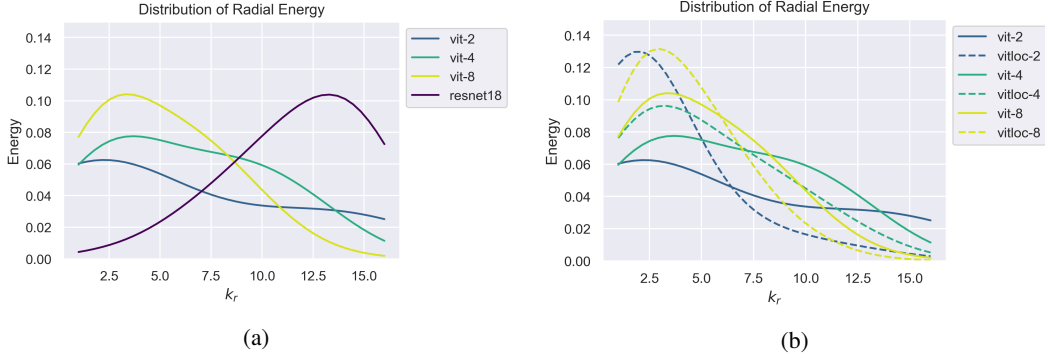


Figure 4: Radial Energy of the Adversarial Perturbations of Vision Transformer and Local Vision Transformer models. (a) All Vision Transformer models (vit-2, vit-4, vit-8) have more energy in lower frequencies than ResNet18. (b) Locally Connected model’s (vitloc-2, vitloc-4, vitloc-8) spectrum have more energy in lower frequencies compared to their standard ViT counterpart.

In addition to these results, we tested the high frequency bias of the bounded-width parametrization. By performing a new variant of the hidden features experiment, we now localize the information in the low, medium, or high frequencies by introducing the same class-dependent signal in concentric rings in those corresponding frequencies on the spectrum of the training and testing set of CIFAR10 (See Methods).

Table 2: Performance on CIFAR-10 on base vs frequency-based dataset. Low Frequency ( $\epsilon = 0.5$ ), Medium Frequency ( $\epsilon = 5e - 02$ ) and High Frequency ( $\epsilon = 5e - 04$ ). Different  $\epsilon$ ’s were chosen to match the signal to noise ratio of those frequencies bands and make the task as difficult as possible. Standard Deviation was calculated over 5 runs.

Models	Low Frequency	Medium Frequency	High Frequency
Full-Width Convolution (L=1)	100.0	41.03	41.38
Full-Width Convolution (L=3)	100.0	39.80	40.97
Bounded-Width Convolution (L=1)	100.0	49.99	53.60
Bounded-Width Convolution (L=3)	100.0	94.17	98.47
Fully Connected (L=1)	99.78	41.45	41.38
Fully Connected (L=3)	100.0	46.37	41.21
Locally Connected (L=1)	100.0	44.39	46.23
Locally Connected (L=3)	100.0	47.36	54.73

In Table 2, we can see the performance of the linear models with this new frequency-based class-dependent features. We observe that all models are able to use the low-frequency shortcut features in order to perform the task. Furthermore, when the cheat signal is introduced in the medium and high frequencies the full-width convolutional, fully connected, and locally connected models have a much more difficult time in selecting this signal. Where the Bounded-Width Convolutional Model is able to perform the best in medium and high frequencies compared to the other models and this difference is also maintained with larger depth.

**Vision Transformers do not exhibit a high frequency bias.** Since local convolutions cause a bias towards high frequency features and adversarial perturbations, it is natural to ask: Are high-performance deep models without convolutions less biased towards high-frequency features? One possible architecture is the Vision Transformer (ViT), which has performed on par with convolution-based architectures in many tasks including object recognition [28]. Furthermore, recent work has shown that ViTs can be more robust to high frequency adversarial perturbations than ResNets [29].

We hypothesize that the lack of convolutional operations in ViTs is responsible for this greater robustness to high frequency attacks. In order to test this, we trained a ViT with different patch sizes on CIFAR-10 (See Supp. Sec. B.4 for training details). All of these models achieved about 80% test accuracy. Then, we attacked these models with a PGD-Linf attack, the same used earlier in the paper. In Figure 4a, we observe the average frequency spectrum of ViTs with different word/patch sizes

( $2 \times 2$ ,  $4 \times 4$ ,  $8 \times 8$ ), as compared to a ResNet18 with similar test accuracy (we stopped the training when the model had near 80% test accuracy). We observe that all of the ViTs have more energy in the lower frequencies than the ResNet18. This strongly suggests that the robustness to high frequency attacks shown in [29] might be due to the lack of convolution layers. Furthermore, we observe that different patch/word sizes also have an impact on the spectrum, with smaller word sizes producing higher frequency spectra. This is consistent with the theoretical and empirical results comparing full-width and bounded-width convolutional models.

However, as others have suggested [30], some layers of the ViT can still be interpreted as convolutional layers, so the model is not entirely convolution-free. In particular, the first embedding layer is shared across all image patches, and therefore can be interpreted as a convolutional layer with stride equal to the patch/kernel size. This leads us to ask: Can we remove this layer and shift the energy spectrum to even lower frequencies? To test this we defined a new ViT architecture in which we removed the weight sharing in the first layer patch embedding by using a locally connected layer with the same kernel size and stride as the convolutional version, so that each patch has independent weights. We call this architecture the Visual Local Transformer (ViTLoc). Then, we trained this architecture on CIFAR-10 (see Performance in Sup. Table 7) and computed its adversarial perturbations. In Figure 4b, we observe that every ViTLoc model has a lower frequency spectrum than its ViT counterpart. This is more evidence that avoiding the convolutional parametrization, even in very complex state-of-the-art models, can reduce the high frequency bias, and therefore, high frequency adversarial perturbations.

## Conclusions

We provide both empirical as well as theoretical evidence that one of the causes of the high-frequency adversarial examples is the bounded-width convolutional architecture of modern high-performance CNNs. To this end, we first showed that theoretical results in deep linear full-width convolutional models [15] extend to nonlinear models. In line with these results, we find that the Vision Transformer architecture, which features almost no explicit convolutions, is less biased towards high frequencies. We demonstrated that by removing one of the only convolutional layers in the model (Local Vision Transformer Architecture), this bias can be reduced even further. We think this is important because ViT, similar to ResNets, have multiple components such as Norm Layers, Skip Connections, Attention, etc, that should affect the implicit bias of the model. However, we found that the linear layer parametrization seem to be crucial to the nature of the features learned and therefore for the adversarial perturbations.

Second, we derived new theoretical results for the implicit bias of deep linear bounded-width convolutions, showing that such networks are biased towards high-frequency features. Furthermore, compared to other theories that try to understand the right basis for model generalization [12–14], our work relates this back to the optimization bias due to model parametrization. We think this is a more general framework for understanding why certain neural networks (convolutional neural networks) pick frequency-based features compared to features in other basis. Our work does not claim that all adversarial perturbations contain only high-frequency components. Instead, we show that architectures with local convolutions can be successfully attacked by perturbations that contain more energy in the high frequencies as compared to non-local architectures (e.g. fully connected, locally connected, and Vision Transformers).

Moreover, by a novel steganography experiment, we could clearly confirm that this bias extends to nonlinear models, and that it strongly influences what features can be learned by the models. We think is a new and exciting directions to probe the ability of the model to generalize along any basis not just Fourier. In addition, our work has shown that adversarial perturbations can be an important technique to understand what are the features been learned by a neural networks. This is even the case while the model is learning. In Supplementary Section C, we have shown that the F-principle, which dictates the dynamics of features learned by a neural network are also reflected in the adversarial perturbations found for a model. This is further indication that adversarial analysis will be beneficial for understanding how neural networks operate.

Finally, much work about generalization and adversarial attacks has been centered around bias in datasets[11, 9], however, here we show that attention needs to be paid to bias caused by architectural choices as well. This work is just the start of establishing the relationship between implicit bias due to model parametrization and the robustness of neural networks to different kinds of input perturbations.

We believe this understanding can help drive models towards the most useful set of features and reduce the adversarial susceptibility of modern neural networks.

## Acknowledgments

This research has been funded by the NSF NeuroNex program through grant DBI-1707400. This research was also supported by Intelligence Advanced Research Projects Activity (IARPA) via Department of Interior/Interior Business Center (DoI/IBC) contract number D16PC00003. The U.S. Government is authorized to reproduce and distribute reprints for Governmental purposes notwithstanding any copyright annotation thereon. Disclaimer: The views and conclusions contained herein are those of the authors and should not be interpreted as necessarily representing the official policies or endorsements, either expressed or implied, of IARPA, DoI/IBC, or the U.S. Government.

## Methods

**Neural Network Training.** Each architecture was defined by the number of hidden layers, and nonlinearities (See Supp Table 6). In terms of hyperparameters, we tuned the maximum learning rates for each model by starting from a base learning rate of 0.1, and then, if there were visible failures during training (most commonly, the model converging to chance performance), we adjusted the learning rate up/down by a factor of 10 or 50. Amongst the model architectures we explored, the only hyper-parameter that was tuned was the learning rate. The final values of the learning rates after search are detailed in Table 9. In addition, all the models were trained with linearly decaying learning rate follow 0.3 factor for each epoch and resetting the learning rate back to max when you trained the model at least 20 epochs. All the models were trained on a single GTX 1080 Ti for at least 40 epochs (30 to 120 GPU minutes), and we choose the epoch with the highest accuracy for further experiments (see hyperparameters of training and accuracy on Supp Sec. B.4)

**Adversarial Attack Generation.** We used the Foolbox package [31] (MIT license) to generate adversarial perturbations  $\delta$  for every example in the test set for a fully trained model (PGD-Linf, PGD-L2, PGD-L1 [32], BB-Linf and BB-L2 [33]). Finally, we computed the 2-D Discrete Fourier spectrum  $\hat{\delta} := \mathcal{F}\delta$  of the perturbation  $\delta$ . Details of the attacks are available in Supp. Table 12.

**$\beta$  Calculation and Toeplitz Matrix.** For the computation of  $\beta$ , we used two different methods. For the linear models, we transformed the weights of every architecture into their matrix form. For example for the convolutional operation, we generated a Toeplitz matrix per convolutional filter and then calculated the dot product of the first  $l$  matrices to get the  $\beta_l$  (or for all  $l = 1, \dots, L$  to get the input-output function  $\beta$ ). For the nonlinear models, because the nonlinearities does not allow us to use the weights directly, we decided to use a proxy, the saliency map. Saliency Map is the gradient ( $\frac{df}{dx}$ ) of the function ( $f(x)$ ) with respect to the input image ( $x$ ). In the linear case, these gradients are exactly the weights of the function  $\beta$  (up to a constant), which we confirmed using the Toeplitz computation above. For the nonlinear models, because the weights used changed per example, the gradient gave us a good approximation of those weights.

**Generation of Hidden Shortcut Features.** For each class, we sampled a  $3 \times 32 \times 32$  matrix of scalars from a standard Gaussian distribution with mean of 0 and standard deviation of 1 ( $N_{class}$ ). Then we multiplied this matrix by a scalar factor  $\epsilon$ , which was selected via hyperparameter search. Next, we generated a masking matrix ( $M_{class}$ ) of the same size,  $3 \times 32 \times 32$ . For the sparse shortcut feature experiment this matrix was generated from a Bernoulli distribution with an specific average sparsity level  $\rho$ . For the frequency-based class dependent features, we selected an upper and lower bound radii as a factor of the max frequency (0.1 and 0.2; 0.4 and 0.5; and 0.8 and 0.9 for the low, medium and high frequencies respectively). These were the ranges used to produce the masking matrix  $M_{class}$ . Next, we computed the hardmard product of  $M_{class}$  with  $N_{class}$ . Then, this class-specific shortcut feature was added into the Fourier spectrum of CIFAR-10 train and test images corresponding to their respective classes. The mathematical definitions are as follows:

$$\begin{aligned}
N_{\text{class}} &\sim \mathcal{N}(0, 1) \\
M_{\text{class}} &= \begin{cases} \text{Sparse} & M_{\text{class}} \sim \text{Bernoulli}(\rho) \\ \text{Frequency} & M_{\text{class}} = \begin{cases} \text{Inside frequency range} & 1 \\ \text{Outside frequency range} & 0 \end{cases} \end{cases} \\
\eta_{\text{class}} &= M_{\text{class}} \odot (\epsilon * N_{\text{class}}), \quad \widehat{x} = \widehat{x} + \eta_{\text{class}}.
\end{aligned}$$

## References

- [1] Justin Gilmer, Luke Metz, Fartash Faghri, Samuel S Schoenholz, Maithra Raghu, Martin Wattenberg, and Ian Goodfellow. Adversarial spheres. *arXiv preprint arXiv:1801.02774*, 2018.
- [2] Saeed Mahloujifar, Dimitrios I Diochnos, and Mohammad Mahmoody. The curse of concentration in robust learning: Evasion and poisoning attacks from concentration of measure. In *Proceedings of the AAAI Conference on Artificial Intelligence*, volume 33, pages 4536–4543, 2019.
- [3] Thomas Tanay and Lewis Griffin. A boundary tilting perspective on the phenomenon of adversarial examples. *arXiv preprint arXiv:1608.07690*, 2016.
- [4] Nic Ford, Justin Gilmer, Nicolas Carlini, and Dogus Cubuk. Adversarial examples are a natural consequence of test error in noise. *arXiv preprint arXiv:1901.10513*, 2019.
- [5] Alhussein Fawzi, Hamza Fawzi, and Omar Fawzi. Adversarial vulnerability for any classifier. In *Advances in Neural Information Processing Systems*, pages 1178–1187, 2018.
- [6] Sébastien Bubeck, Eric Price, and Ilya Razenshteyn. Adversarial examples from computational constraints. *arXiv preprint arXiv:1805.10204*, 2018.
- [7] Ian J Goodfellow, Jonathon Shlens, and Christian Szegedy. Explaining and harnessing adversarial examples. *arXiv preprint arXiv:1412.6572*, 2014.
- [8] Ludwig Schmidt, Shibani Santurkar, Dimitris Tsipras, Kunal Talwar, and Aleksander Madry. Adversarially robust generalization requires more data. In *Advances in Neural Information Processing Systems*, pages 5014–5026, 2018.
- [9] Andrew Ilyas, Shibani Santurkar, Dimitris Tsipras, Logan Engstrom, Brandon Tran, and Aleksander Madry. Adversarial examples are not bugs, they are features. In *Advances in Neural Information Processing Systems*, pages 125–136, 2019.
- [10] Dong Yin, Raphael Gontijo Lopes, Jon Shlens, Ekin Dogus Cubuk, and Justin Gilmer. A fourier perspective on model robustness in computer vision. In *Advances in Neural Information Processing Systems*, pages 13255–13265, 2019.
- [11] Haohan Wang, Xindi Wu, Zeyi Huang, and Eric P Xing. High-frequency component helps explain the generalization of convolutional neural networks. In *Proceedings of the IEEE/CVF Conference on Computer Vision and Pattern Recognition*, pages 8684–8694, 2020.
- [12] Yusuke Tsuzuku and Issei Sato. On the structural sensitivity of deep convolutional networks to the directions of fourier basis functions. In *Proceedings of the IEEE/CVF Conference on Computer Vision and Pattern Recognition*, pages 51–60, 2019.
- [13] Guillermo Ortiz-Jimenez, Apostolos Modas, Seyed-Mohsen Moosavi-Dezfooli, and Pascal Frossard. Hold me tight! influence of discriminative features on deep network boundaries. *arXiv preprint arXiv:2002.06349*, 2020.
- [14] Guillermo Ortiz-Jimenez, Apostolos Modas, Seyed-Mohsen Moosavi-Dezfooli, and Pascal Frossard. Neural anisotropy directions. *arXiv preprint arXiv:2006.09717*, 2020.

- [15] Suriya Gunasekar, Jason D Lee, Daniel Soudry, and Nati Srebro. Implicit bias of gradient descent on linear convolutional networks. In *Advances in Neural Information Processing Systems*, pages 9461–9471, 2018.
- [16] Chulhee Yun, Shankar Krishnan, and Hossein Mobahi. A unifying view on implicit bias in training linear neural networks. *arXiv preprint arXiv:2010.02501*, 2020.
- [17] Justin Sahs, Aneel Damaraju, Ryan Pyle, Onur Tavaslioglu, Josue Ortega Caro, Hao Yang Lu, and Ankit Patel. A functional characterization of randomly initialized gradient descent in deep re{lu} networks, 2020. URL <https://openreview.net/forum?id=BJ19PRVKDS>.
- [18] Francis Williams, Matthew Trager, Daniele Panozzo, Claudio Silva, Denis Zorin, and Joan Bruna. Gradient dynamics of shallow univariate relu networks. In *Advances in Neural Information Processing Systems*, pages 8376–8385, 2019.
- [19] Blake Woodworth, Suriya Gunasekar, Jason D Lee, Edward Moroshko, Pedro Savarese, Itay Golan, Daniel Soudry, and Nathan Srebro. Kernel and rich regimes in overparametrized models. *arXiv preprint arXiv:2002.09277*, 2020.
- [20] Justin Sahs, Ryan Pyle, Aneel Damaraju, Josue Ortega Caro, Onur Tavaslioglu, Andy Lu, and Ankit Patel. Shallow univariate relu networks as splines: Initialization, loss surface, hessian, & gradient flow dynamics. *arXiv preprint arXiv:2008.01772*, 2020.
- [21] Zhiyuan Li, Ruosong Wang, Dingli Yu, Simon S Du, Wei Hu, Ruslan Salakhutdinov, and Sanjeev Arora. Enhanced convolutional neural tangent kernels. *arXiv preprint arXiv:1911.00809*, 2019.
- [22] Sanjeev Arora, Simon S Du, Wei Hu, Zhiyuan Li, Russ R Salakhutdinov, and Ruosong Wang. On exact computation with an infinitely wide neural net. In *Advances in Neural Information Processing Systems*, pages 8139–8148, 2019.
- [23] Alex Krizhevsky, Geoffrey Hinton, et al. Learning multiple layers of features from tiny images. 2009.
- [24] Adam Paszke, Sam Gross, Francisco Massa, Adam Lerer, James Bradbury, Gregory Chanan, Trevor Killeen, Zeming Lin, Natalia Gimelshein, Luca Antiga, et al. Pytorch: An imperative style, high-performance deep learning library. *Advances in neural information processing systems*, 32:8026–8037, 2019.
- [25] Aleksander Madry, Aleksandar Makelov, Ludwig Schmidt, Dimitris Tsipras, and Adrian Vladu. Towards deep learning models resistant to adversarial attacks. *arXiv preprint arXiv:1706.06083*, 2017.
- [26] Gabriel Goh. A discussion of ‘adversarial examples are not bugs, they are features’: Two examples of useful, non-robust features. *Distill*, 2019. doi: 10.23915/distill.00019.3. <https://distill.pub/2019/advex-bugs-discussion/response-3>.
- [27] Abbas Cheddad, Joan Condell, Kevin Curran, and Paul Mc Kevitt. Digital image steganography: Survey and analysis of current methods. *Signal processing*, 90(3):727–752, 2010.
- [28] Alexey Dosovitskiy, Lucas Beyer, Alexander Kolesnikov, Dirk Weissenborn, Xiaohua Zhai, Thomas Unterthiner, Mostafa Dehghani, Matthias Minderer, Georg Heigold, Sylvain Gelly, et al. An image is worth 16x16 words: Transformers for image recognition at scale. *arXiv preprint arXiv:2010.11929*, 2020.
- [29] Rulin Shao, Zhouxing Shi, Jinfeng Yi, Pin-Yu Chen, and Cho-Jui Hsieh. On the adversarial robustness of visual transformers. *arXiv preprint arXiv:2103.15670*, 2021.
- [30] Zhengsu Chen, Lingxi Xie, Jianwei Niu, Xuefeng Liu, Longhui Wei, and Qi Tian. Visformer: The vision-friendly transformer. *arXiv preprint arXiv:2104.12533*, 2021.
- [31] Jonas Rauber, Wieland Brendel, and Matthias Bethge. Foolbox: A python toolbox to benchmark the robustness of machine learning models. *arXiv preprint arXiv:1707.04131*, 2017.
- [32] Alexey Kurakin, Ian Goodfellow, and Samy Bengio. Adversarial examples in the physical world. *arXiv preprint arXiv:1607.02533*, 2016.

- [33] Wieland Brendel, Jonas Rauber, Matthias Kümmerer, Ivan Ustyuzhaninov, and Matthias Bethge. Accurate, reliable and fast robustness evaluation. In *Advances in Neural Information Processing Systems*, pages 12861–12871, 2019.
- [34] Zhi-Qin John Xu, Yaoyu Zhang, and Yanyang Xiao. Training behavior of deep neural network in frequency domain. In *International Conference on Neural Information Processing*, pages 264–274. Springer, 2019.
- [35] Saifallah Ghobber and Philippe Jaming. On uncertainty principles in the finite dimensional setting. *Linear algebra and its applications*, 435(4):751–768, 2011.

# A Supplementary Material

## A.1 Figures

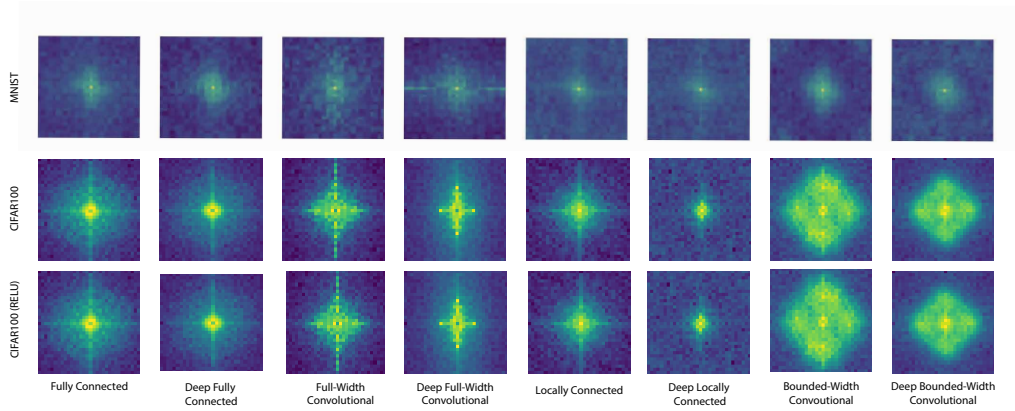


Figure 5: Adversarial Spectrum for: Fully Connected, Deep Fully Connected, Full-Width Convolutional, Deep Full-Width Convolutional, Locally Connected, Deep Fully Connected, Bounded-Width Convolutional, Deep Bounded Width Convolutional models for MNIST (Linear Models), CIFAR100 (Linear Models) and CIFAR100 (NonLinear Models). Both CIFAR100 results are similar to the CIFAR10 experiments. No difference between MNIST models, which reflects that MNIST is mainly composed of low frequency features

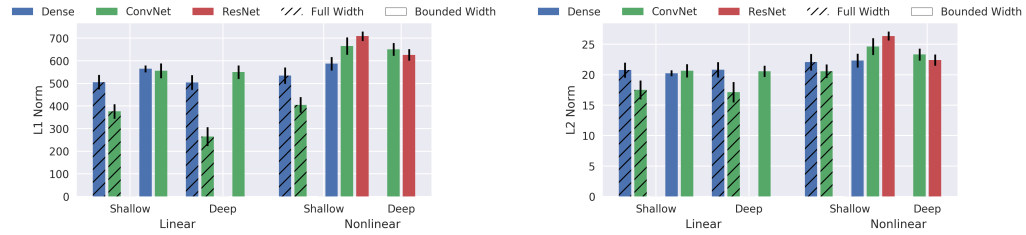


Figure 6: Comparison of Adversarial Perturbation Norms  $\|\hat{\delta}\|_p$  for  $p = 1, 2$  for different linear and nonlinear models. The relations between norms of nonlinear models mirror and accentuate those of linear models. See Results for detailed comparisons.

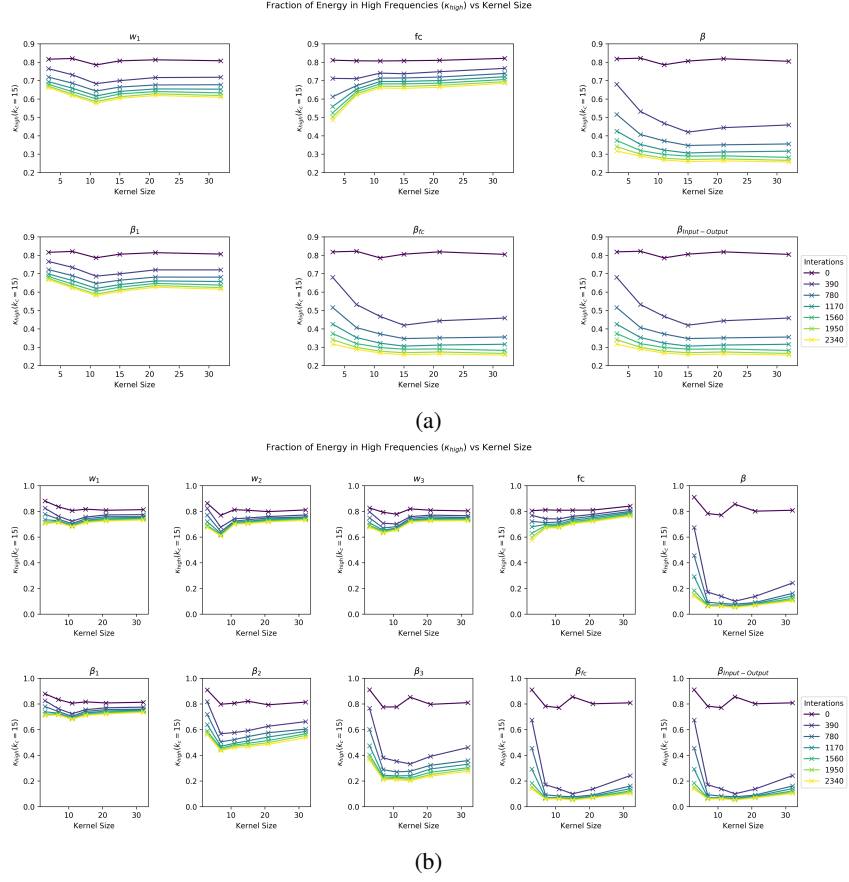


Figure 7: Concentration of energy  $\kappa_{high}$  for  $\kappa_r = 15$  for each  $\beta_l$  for all  $l$  versus kernel size (3,7,9,11,15, 21, or 32). All models were trained for 40 epochs on Grayscale CIFAR10. (a) One hidden layer models (b) Three hidden layer models.

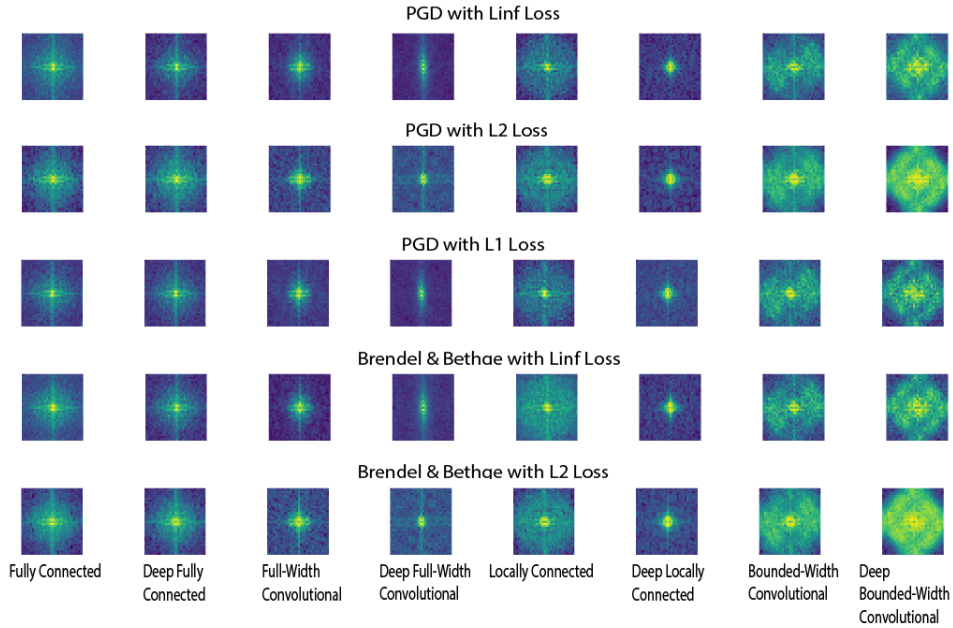


Figure 8: Average Adversarial Perturbation Fourier Spectrum for Fully Connected, Full-Width, Locally Connected and Bounded-Width **Linear** models.

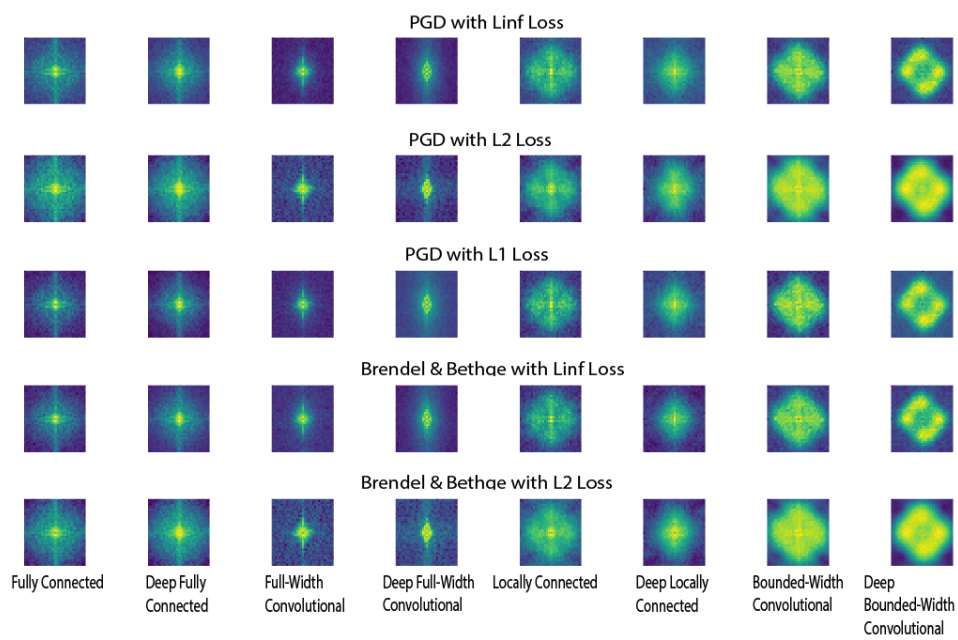


Figure 9: Average Adversarial Perturbation Fourier Spectrum for Fully Connected, Full-Width, Locally Connected and Bounded-Width **NonLinear** models.

## A.2 Tables

Table 3: Spearman Correlation between Fourier spectrum of Delta and Beta for different models.

Model	Spearman Correlation of $\hat{\beta}$ and $\hat{\delta}$	
	Linear Model	Nonlinear Model
Fully Connected	0.353	0.439
Deep Fully Connected	0.343	0.504
Full Width Convolutional	0.276	0.327
Deep Full Width Convolutional	0.272	0.452
Locally Connected Linear	0.240	0.275
Bounded Width Convolutional	0.266	0.371
Deep Bounded Width Convolutional	0.306	0.344

Table 4: Frequency-Domain Norms of Predictor  $\hat{\beta}$  and Adv. Pert.  $\hat{\delta}$  for Linear Models. With Equivalent performance (See Sup Figure 7), Convolutional Models have smaller  $\|\hat{\beta}\|_1$ , supporting the implicit Fourier hypothesis.

Model	$\ \hat{\delta}\ _2$	$\ \hat{\delta}\ _1$	$\ \hat{\beta}\ _2$	$\ \hat{\beta}\ _1$
Fully Connected	20.77 $\pm$ 1.23	505.95 $\pm$ 32.22	546.89 $\pm$ 43.37	2232.46 $\pm$ 166.27
Full Width Convolution	17.52 $\pm$ 1.56	376.31 $\pm$ 32.66	544.83 $\pm$ 42.40	1598.37 $\pm$ 181.44
Bounded Width Convolution	20.65 $\pm$ 1.09	556.32 $\pm$ 32.64	500.67 $\pm$ 47.46	2623.04 $\pm$ 331.42
Deep Fully Connected	20.83 $\pm$ 1.25	503.92 $\pm$ 32.62	554.16 $\pm$ 38.95	2168.06 $\pm$ 134.07
Deep Full Width Convolution	17.13 $\pm$ 1.68	265.40 $\pm$ 41.72	522.99 $\pm$ 39.72	1417.68 $\pm$ 213.91
Deep Bounded Width Convolution	20.57 $\pm$ 0.94	550.30 $\pm$ 29.71	498.52 $\pm$ 47.15	2392.09 $\pm$ 278.55

Table 5: Frequency-Domain Norms of Adv. Pert.  $\hat{\delta}$  for Nonlinear Models. With similar performance (Supp. Table 4), Full Width and Bounded Width convolutional models produce adversarial attacks with smaller  $\|\hat{\delta}\|_1$ .

Model	$\ \hat{\delta}\ _2$	$\ \hat{\delta}\ _1$
Fully Connected	22.06 $\pm$ 1.35	534.34 $\pm$ 35.93
Locally Connected	22.32 $\pm$ 1.13	587.61 $\pm$ 29.89
Full Width Convolution	20.57 $\pm$ 1.11	405.49 $\pm$ 34.16
Bounded Width Convolution	24.63 $\pm$ 1.36	665.22 $\pm$ 38.55
Shallow ResNet	26.36 $\pm$ 0.74	709.06 $\pm$ 20.76
VGG19	23.32 $\pm$ 0.99	650.73 $\pm$ 27.87
ResNet18	22.42 $\pm$ 0.91	626.60 $\pm$ 25.40

## B Experimental Details

### B.1 Model Architecture

Table 6: Model Architectures

Model Architecture	# Hidden Layers	Nonlinearity	Channels
Fully Connected	1,3	None, ReLU	3072
Bounded Width Convolution	1,3	None, ReLU	32
Full Width Convolution	1,3	None, ReLU	32
Locally Connected	1,3	None, ReLU	32

### B.2 Model Performance

Table 7: Test Accuracy for all models trained on CIFAR-10. All linear models have similar performance. Nonlinear models exhibit more variability.

Model Architecture	Test Accuracy
Fully Connected (Linear)	41%
Locally Connected (Linear)	35%
Full Width Convolution (Linear)	41%
Bounded Width Convolution (Linear)	41%
Deep Fully Connected (Linear)	41%
Deep Full Width Convolution (Linear)	36%
Deep Bounded Width Convolution (Linear)	41%
Fully Connected (NonLinear)	52%
Full-Width Convolution (NonLinear)	52%
Locally Connected (NonLinear)	54%
Bounded Width Convolution (NonLinear)	63%
ViT-2	79.8%
ViT-4	80.1%
ViT-8	78.4%
ViTLoc-2	75.3%
ViTLoc-4	80.2%
ViTLoc-8	74.5%
ResNet18	92%

### B.3 Adversarial Attack Success

Table 8: Adversarial Success for all models trained on CIFAR-10. All values are shown for PGD-Linf of B.5

Model Architecture	Adversarial Success (PGD-Linf)
Fully Connected (Linear)	100.0%
Locally Connected (Linear)	100.0%
Full Width Convolution (Linear)	100.0%
Bounded Width Convolution (Linear)	100.0%
Deep Fully Connected (Linear)	100.0%
Deep Full Width Convolution (Linear)	100.0%
Deep Bounded Width Convolution (Linear)	100.0%
Fully Connected (NonLinear)	100.0%
Full-Width Convolution (NonLinear)	100.0%
Locally Connected (NonLinear)	100.0%
Bounded Width Convolution (NonLinear)	100.0%
ViT-2	100.0%
ViT-4	99.7%
ViT-8	100.0%
ViTLoc-2	100.0%
ViTLoc-4	100.0%
ViTLoc-8	99.9%
ResNet18	100.0%

All adversarial attacks were performed on a single GTX 1080 Ti for all 10 thousand testset images.

### B.4 Training Hyperparameters

Table 9: Learning rates for the various models considered on CIFAR-10. All other hyper-parameters were fixed.

Model Architecture	Learning Rate	Batch Size	Learning Rate Drop
Bounded Width Convolution	.01	128	Yes
Fully Connected	.01	128	Yes
Locally Connected	.01	128	Yes
Full Width Convolution	.002	128	Yes
Bounded Width Convolution	.002	128	Yes

Table 10: Learning rates for the various models considered on CIFAR-100. All other hyper-parameters were fixed.

Model Architecture	Learning Rate	Batch Size	Learning Rate Drop
Bounded Width Convolution	.01	128	Yes
Fully Connected	.01	128	Yes
Locally Connected	.01	128	Yes
Full Width Convolution	.002	128	Yes
Bounded Width Convolution	.002	128	Yes

### B.5 Adversarial Attack Configurations

**Learning Rates.** All the models adversarial attacks were generated using the configuration above with the Foolbox package [31].

Table 11: Learning rates for the various models considered on MNIST. All other hyper-parameters were fixed.

Model Architecture	Learning Rate	Batch Size	Learning Rate Drop
Bounded Width Convolution	.01	100	Yes
Fully Connected	.01	100	Yes
Locally Connected	.01	100	Yes
Full Width Convolution	.002	100	Yes
Bounded Width Convolution	.002	100	Yes

Table 12: Adversarial Attack hyperparameters

Attack	Metric	Learning Rate	Number of Steps	Max Norm, $\epsilon$
Projected Gradient Descent	$L_\infty$	0.1	1000	8.0/255.0
Projected Gradient Descent	$L_2$	0.1	1000	2.0
Projected Gradient Descent	$L_1$	0.1	200	0.1
Brendel-Bethge Attack	$L_\infty$	1e-03	1000	-
Brendel-Bethge Attack	$L_2$	1e-03	1000	-

## C Dynamics of Adversarial Examples in Frequency Domain

We have observed that adversarial perturbations reflect the type of features learned by the model. We propose that this is an interesting lens to understand more broadly what are neural networks learning. For example, one theory related to feature learning on neural networks is the F-principle [34]. This work found that deep neural networks first learned low frequency features and then move towards high frequency features. Here we hypothesize that this low to high frequency feature learning during training should be reflected on the adversarial perturbations a model is sensitive to at any given point during learning. This will be further evidence that adversarial perturbations are a reflection of the function learned by the model but not just spurious correlations. In order to test this hypothesis, we trained a ResNet18 model on the CIFAR-10 dataset [23] (MIT) using PyTorch [24]. Then, we used the Foolbox package [31] (MIT) to generate adversarial attacks for every example in the test set for intermediate models during training, via an  $\ell_\infty$  Projected Gradient Descent attack [32] (see Supplementary Sec. B.5). In Sup. Figure 10, we see the evolution of the frequency spectrum of the adversarial perturbations: early in training the adversarial perturbations tend to contain low frequencies (with higher norms), and as training progresses, there is a consistent evolution towards higher frequencies (with lower norms). Thus, adversarial perturbations evolve through learning to higher frequencies and lower amplitudes.

This phenomenon is also confirmed in Sup. Figures 11a and 11b. Here, we observe the marginal radial and angular distributions  $E(k_r), E(k_\phi)$  of the energy spectrum  $E(k_r, k_\phi) := |\widehat{\delta}(k_r \cos k_\phi, k_r \sin k_\phi)|_{\mathbb{C}}^2$ , where  $(k_r, k_\phi)$  denotes polar coordinates in the frequency domain. We also observe that (i) the radial energy distribution shifts from low to high frequency, and (ii) the angular energy distribution becomes more uniform (ring structure). The evolution of the adversarial perturbations in the frequency domain shows an optimization bias of state-of-the-art convolutional models to frequency-based features.

## D Formal Proofs of High Frequency Bias

**Theorem 1.** *Let  $\beta := \star_{l=1}^{L-1} w_l$  be the end to end linear predictor. Then spatially concentrating the energy of each convolutional filter  $w_l \in \mathbb{R}^D$  results in an increased concentration of energy in high frequencies for  $\widehat{\beta}$ .*

*Proof.* Let us first concentrate on a single convolutional filter  $w_l \in \mathbb{R}^D$ . Given an arbitrary choice of frequency interval  $\Omega := \{-k, \dots, 0, \dots, +k\}$  and space interval  $S := \{-a, \dots, 0, \dots, +a\}$ , we want to prove that reducing the energy fraction in the complementary set  $S^c$  implies that we must increase the energy fraction in the complementary set  $\Omega^c$ . The result follows from a direct

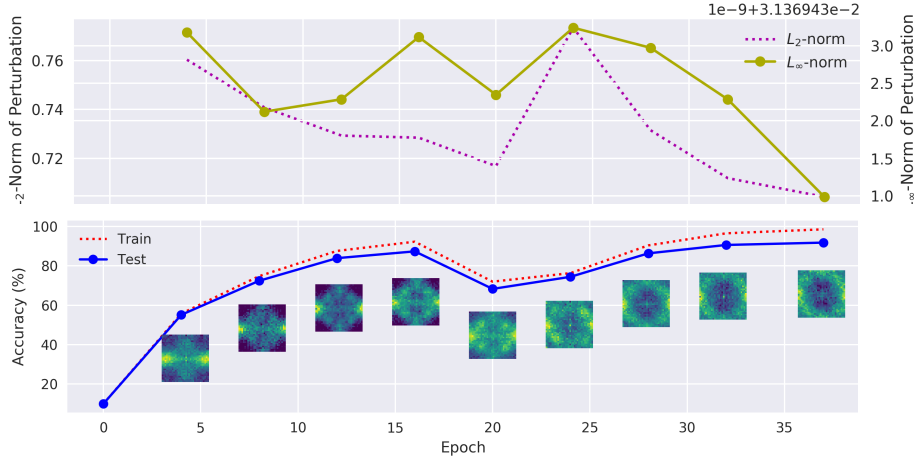


Figure 10: Top: Dynamics of  $\ell_2$  and  $\ell_\infty$  norms of the adversarial perturbations ( $\delta$ ) during training of ResNet18. Over training, adversarial perturbations become smaller in amplitude (the norm increase after around 20 epochs is due to learning rate reset which decreases performance). Bottom: Evolution of the adversarial perturbation spectrum ( $\hat{\delta}$ ) over training. The adversarial perturbation spectrum evolves from low-frequencies to high frequencies as performance increases.



Figure 11: (a) Distribution of radial energy  $k_r$  of the Fourier spectrum of adversarial perturbations. (b) Distribution of angular energy  $k_\phi$  (in degree) of the Fourier spectrum of adversarial perturbations. We observe an evolution of adversarial perturbations over training from lower to higher frequencies for the ResNet18 model, and from certain directions to all directions uniformly.

application of the Uncertainty Principle for finite-dimensional vector spaces, as shown e.g. in Ghobber-Jaming [35]. In particular let  $\{\widehat{\beta}_i\}_{i=1}^D$  be the coefficients of the Discrete Fourier Transform (DFT) From equation 1.2 in [35] we have

$$\|w\|_{\ell^2(S^c)} + \|\widehat{w}\|_{\ell^2(\Omega^c)} \geq \|w\|_2 C(S, \Omega) \quad (1)$$

where  $C(S, \Omega)$  is constant when the intervals  $S, \Omega$  are fixed. Dividing both sides of the inequality by  $\|w\|_2$  we have

$$\kappa(S^c) + \widehat{\kappa}(\Omega^c) \geq \text{const}$$

where  $\kappa(\mathcal{A}) := \|w\|_{\ell^2(\mathcal{A})}/\|w\|_2$  is the spatial energy concentration of  $w$  in the index set  $\mathcal{A}$  and  $\widehat{\kappa}(\mathcal{B})$  is the analogous quantity for  $\widehat{w}$ . Thus increasing the energy concentration in the spatial interval  $S$  will decrease it in  $S^c$  and by the inequality above increases  $\kappa(\Omega^c)$ . In other words, considering  $\Omega$  to be the low frequencies, there will be an increase in the high frequency energy concentration.

The reasoning above can be extended from a single convolutional filter to the full end-to-end weights vector,  $\beta := \star_{l=1}^{L-1} w_l$ , as follows. Note first that, using the convolution theorem, the Discrete Fourier transform of  $\beta$  is the Hadamard product of the Discrete Fourier transforms of the per-layer weights  $w_l$  i.e.

$$\widehat{\beta} = \widehat{w}_{L-1} \odot \cdots \odot \widehat{w}_1.$$

Let us consider the Fourier energy in the low frequency  $\Omega$ :

$$\widehat{\beta}_\Omega = \widehat{w}_{L-1,\Omega} \odot \cdots \odot \widehat{w}_{1,\Omega}.$$

Taking the  $\ell_2$  norm and using the inequality  $\|a \odot b\|_2 \leq \|a\|_2 \|b\|_2$  multiple times we can then write

$$\kappa(\Omega, \beta) \leq \prod_{l=1}^{L-1} \kappa(\Omega, w_l).$$

Let us now decrease the energy content in each spatial domain  $S$  of the filters  $w_l$ . By the reasoning above this will increase the energy content in Fourier domain in the intervals  $\Omega^c$  i.e. decrease each  $\kappa(\Omega, w_l)$ . By the last inequality this will decrease  $\kappa(\Omega, \beta)$ , i.e. increase the energy in the high frequency domain ( $\Omega^c$ ) in  $\beta$ .  $\square$

**Lemma 2.** *Concentrating the kernel energy in spatial domain increases the implicit regularization term in the optimization in [Gunasekar]:*

$$\forall a' < a : R_{BWC;a'}(\beta) \geq R_{BWC;a}(\beta)$$

*Proof.* Reducing filter size  $K$  will increase energy in high freqs i.e.  $\forall K' < K : \kappa_{high}(\beta; K') > \kappa_{high}(\beta; K)$ . This means that the space-limiting constraints only grow more stringent as we reduce  $K$ , implying that the result of the optimization problem for the implicit regularizer will only increase in cost i.e.  $\forall K' < K : R_{BWC;K'}(\beta) \geq R_{BWC;K}(\beta)$  for any candidate linear predictor  $\beta$ . (Note that this does not refer to the learned features  $\beta^*$  which actually depends on the training data as well). In summary, all else being equal, reducing the kernel size  $K$  causes/induces a bias towards more concentration of energy in higher frequencies in  $\beta$ .  $\square$

In summary reducing the kernel size causes/induces a bias towards more concentration of energy in higher frequencies in  $\beta$ .